Frequency transitions in odor-evoked neural oscillations

Iori Ito[1], **Maxim Bazhenov**[2], **Rose Chik-ying Ong**[1,3], **Baranidharan Raman**[1,4], and **Mark Stopfer**[1,*]

[1]NICHD, NIH, Bethesda, MD

[2]Department of Cell Biology and Neuroscience, University of California, Riverside, CA 92521

[3]Department of Biochemistry, The Chinese University of Hong Kong, HONG KONG

[4]NIST, Gaithersburg, MD.

Summary

In many species sensory stimuli elicit the oscillatory synchronization of groups of neurons. What determines the properties of these oscillations? In the olfactory system of the moth we found that odors elicited oscillatory synchronization through a neural mechanism like that described in locust and *Drosophila*. During responses to long odor pulses, oscillations suddenly slowed as net olfactory receptor neuron (ORN) output decreased; thus, stimulus intensity appeared to determine oscillation frequency. However, changing the concentration of the odor had little effect upon oscillatory frequency. Our recordings *in vivo* and computational models based on these results suggested the main effect of increasing odor concentration was to recruit additional, less well-tuned ORNs whose firing rates were tightly constrained by adaptation and saturation. Thus, in the periphery, concentration is encoded mainly by the size of the responsive ORN population, and oscillation frequency is set by the adaptation and saturation of this response.

Introduction

Sensory stimulus-evoked neural oscillations have been described in many animals (Adrian, 1942; Bresseler and Freeman, 1980; Galambos et al., 1981; Gray et al., 1989; Laurent and Naraghi, 1994; Stopfer et al., 1997; Schadow et al., 2007; Tanaka et al., 2009). For a particular modality in a given species, oscillation frequency often seems unrelated to stimulus intensity. In the locust olfactory system, for example, odors elicit ~20 Hz oscillations that vary little in frequency even when odor concentration varies over 5 orders of magnitude (Stopfer et al., 2003; Assisi et al., 2007). In some cases, though, stimulus intensity does appear to modulate oscillation frequency; the changing velocity of a visual stimulus, for example, can systematically change the frequency of gamma oscillations in the cat visual cortex (Gray and Prisco, 1997). What determines the frequencies of these oscillations?

Here, we used the insect olfactory system to clarify the encoding of odor intensity, and the relationship between stimulus intensity and oscillation frequency. In insects, odor molecules are first detected by olfactory receptor neurons (ORNs). Axons from ORNs converge upon glomeruli in the antennal lobe (AL, analogous to the olfactory bulb) where excitatory projection neurons (PNs, analogous to mitral cells) and mainly inhibitory local interneurons (LNs) interact. PNs send excitatory inputs to LNs, and LNs send rapid inhibitory feedback to PNs via GABA$_A$-like receptors. In locusts, honeybees and *Drosophila*, this feedback circuit has

*Correspondence: stopferm@mail.nih.gov; National Institute of Child Health and Human Development, US National Institutes of Health, Building 35, Room 3A-102, Bethesda, Maryland 20892, USA..

been shown to synchronize groups of PNs, resulting in regular oscillating waves of output that depolarize Kenyon cells (KCs), the intrinsic neurons of the mushroom body (MB). These waves can be detected as a local field potential (LFP; Laurent and Naraghi, 1994; Stopfer et al., 1997; Tanaka et al., 2009).

We found that odors evoked oscillatory responses in the moth *Manduca sexta* much like those described in the locust, honeybee and fly. Further, in the moth, we found that lengthy odor pulses evoked oscillations that began at ~40 Hz but then suddenly decreased to ~15-20 Hz. Simultaneous LFPs and recordings from the moth's antenna (electroantennogram, EAG) showed the net response intensity of ORNs decreased in parallel to the shift in oscillation frequency. This suggested oscillation frequency might be determined by the intensity of the response of the ORN population. In apparent contradiction, though, we also found that odor-evoked oscillation frequency remained remarkably constant across a broad range of odor concentrations. What then is the relationship between stimulus intensity and oscillation frequency?

Our approach, combining experimental and computational methods, led to several conclusions. First, we found the frequency of odor-evoked oscillations in the moth olfactory system is determined by the intensity of input to the oscillatory AL network, but this intensity is determined by sensory adaptation and saturation of ORNs rather than by the intensity of olfactory stimuli. Second, extending prior work, we demonstrated that the vast majority of olfactory dynamic range is encoded in the periphery by the number of responsive ORNs rather than by the firing rates of those ORNs. And third, we characterized a new stable oscillatory regime in which principle neurons participating in an oscillatory network can fire much faster than the oscillation frequency.

Results

Odors evoke fast and then slow LFP oscillations in the MB

To characterize the moth olfactory system's neural responses, we delivered a variety of odors (non-pheromones, see Experimental Procedures) over a wide range of concentrations, and a range of durations from 100 ms (as moths might experience while flying in an odor plume), to 4 s (as moths might experience when sampling food from flowers).

All odor stimuli in our panel induced robust oscillations in the LFP recorded in the MB calyx (a target of PNs, Figure 1A). Figure 1B shows an example of oscillations elicited by a presentation of dilute benzyl alcohol vapor to the ipsilateral antenna of a moth that was mostly intact but with its brain exposed for electrophysiological recording (see Experimental Procedures). The first of a series of odor presentations typically elicited only weak oscillations in the LFP; however, oscillatory power increased rapidly over the first 4 or 5 presentations (Figure S1). Odor pulses briefer than ~1 s elicited fast, 30-40 Hz oscillations in the moth MB; notably, odor pulses longer than ~1 s produced oscillations that were initially fast but then dramatically slowed to 10-20 Hz (Figure 1C-E). Others (Laurent and Davidowitz, 1994; Perez-Orive et al., 2002; Perez-Orive, 2004) and we (Figure S2) had previously observed similar but less pronounced decreases in LFP oscillation frequency in the locust.

LFP oscillations are generated in the AL

Where, and by what mechanism are the oscillations generated? In the moth, we made simultaneous recordings of LFPs from the AL and the MB. All odors we tested induced both fast and slow oscillations in both the AL and the MB; further, the AL-LFP and MB-LFP signals were highly coherent (n=10, Figure 1F).

We next made simultaneous intracellular recordings from pairs of AL neurons together with LFP recordings from the MB (Figure 2; all neurons morphologically identified by dye injection and subsequent confocal imaging). Figure 2A shows an example of a simultaneous recording of the MB-LFP, a PN, and an LN. For most oscillation cycles, a spike in the PN was closely followed (within ~2 ms) in the LN by either a single spike or an EPSP, suggesting LNs received odor-driven periodic input from PNs. And, reciprocally, the membrane potential of this PN revealed a periodic hyperpolarization and depolarization after each spike, suggesting IPSPs from the inhibitory LNs regulated the timing of spikes in the PN. Sliding-window cross-correlations showed that the membrane potential fluctuations in this LN and PN were tightly coupled to LFP oscillations recorded in the MB (spikes clipped; Figure 2B). The oscillations slowed during each trial.

Are the fast and slow oscillations generated in the AL? We made intracellular recordings from 14 PNs and 30 LNs, each simultaneously with LFPs recorded in the MB; Figure 2C displays the spike-LFP phase relationships for spikes pooled from all recorded cells. Spikes in PNs reliably phase-locked to the LFP at a point just past the peak of each cycle during fast (mean direction and 95% confidence interval= $2.79° \pm 9.1°$; 1,950 spikes) and slow ($23.4° \pm 3.3°$; 7,005 spikes) oscillations. Spikes in LNs phase-locked to the LFP just after the PNs during fast ($71.4° \pm 3.0°$; 2,623 spikes) and slow ($72.6° \pm 1.1°$; 12,723 spikes) oscillations. The spike phase distributions of PNs and LNs were each significantly different from uniform distributions (Rayleigh test, $p<0.05$) indicating strong phase-locking. The temporal relationships of these populations match those shown in the simultaneously-recorded example (Figure 2A).

Together, the reliable, periodic relationships among AL neurons suggested that the timed inhibition of PNs by LNs was important for producing synchronous oscillations. To test this, we selectively abolished fast inhibition from LNs to PNs by locally injecting picrotoxin (PCT, a blocker of the $GABA_A$-like inhibition in *Manduca*, Waldrop et al., 1987) into the AL while recording LFPs from the MB. Injection of PCT (n=6) reversibly and significantly reduced odor-evoked fast and slow oscillations; control injections of saline (n=5) had no effect (Figure S3). Thus, inhibition from LNs within the AL is required for the generation of odor-elicited oscillations. Both fast and slow oscillations are generated within the AL and are transmitted to the MB by PNs.

Responses in KCs are shaped by oscillatory input from PNs

To test whether followers of PNs in the MB are sensitive to the oscillatory synchrony of their input, we made intracellular recordings from a set of KCs (n=20, all morphologically identified by dye injection and subsequent confocal imaging).

During odor presentations, the membrane potentials of KCs revealed pronounced sub-threshold fluctuations that were tightly coupled to simultaneously-recorded LFP oscillations. In our four recordings from KCs that revealed sub-threshold activity, peaks of the membrane potential oscillations reliably occurred during falling phases of the LFP oscillation (Figure 3A,B; see Experimental Procedures). Further, odor-evoked spikes in KCs were phase-locked to the falling phases of LFP oscillations during fast ($117.1° \pm 12.2°$; 329 spikes) and slow ($125.7° \pm 5.8°$; 706 spikes) oscillations (Figure 3C). The spike phase distributions for KCs, like those of PNs and LNs, were significantly different from uniform distributions (Rayleigh test, $p<0.05$).

We found that the timing of spikes in PNs, LNs and KCs became more precise (less jitter around the preferred phase) as the oscillation frequency decreased (Figure S4). Together, these results indicated that oscillations strongly influence the timing of spikes in the KCs.

Oscillation frequency remains constant over a wide range of odor concentrations

We had observed that long odor pulses elicited oscillations that shifted dramatically in frequency. What causes this shift? We found that, during long odor pulses, EAGs decreased in amplitude with timing roughly matching that of the frequency shift in the LFP (Figure 1B). The decrease in EAG amplitude was probably caused by sensory adaptation within the ORNs (Kaissling et al., 1987), a mechanism that reduces the intensity of response to an ongoing stimulus. The nearly parallel changes in ORN output intensity and oscillation frequency suggested to us that the intensity of the stimulus may determine oscillation frequency.

To test this, we delivered a wide range of concentrations of three odors (hexanol, octanol and geraniol), expecting to find that higher concentrations elicited more intense responses from ORNs and perhaps faster oscillations in the LFP. Indeed, the range of odor concentrations we used elicited a wide range of responses in the EAG (Figure 4A,B) and in the LFP (Figure S5) from small, near-basal fluctuations to deep, saturating deflections; thus, the range of odor concentrations we used effectively elicited a wide range of response intensities from the population of ORNs. Lower odor concentrations evoked weaker LFP oscillations; higher concentrations evoked stronger oscillations (Figure 4C). However, we found that the initial LFP oscillation frequency remained almost constant across five or more orders of magnitude of odor concentration (Figure 4D). Together, these results appeared contradictory: decreasing drive from ORNs appeared to result in dramatically reduced oscillation frequency, yet experimentally changing the intensity of the input to ORNs had little or no such effect.

The ORN population encodes odor concentration spatially and temporally

The EAG aggregates the responses of many ORNs in the antenna. Thus, we next characterized the responses of individual ORNs on the moth antenna while delivering odor pulses of different concentrations (Figure 5; n=37 ORNs from 9 preparations; see Experimental Procedures). We found that individual responsive ORNs revealed a small dynamic range, firing at rates that varied only within narrow spans of concentration. ORNs responding to moderate odor concentrations (e.g. 0.01%-1% of hexanol; see Experimental Procedures) showed firing rates that quickly saturated (Figure 5F green lines) or even decreased (Figure 5F red lines) as odor concentration increased. And, ORNs that initially responded vigorously to an odor presentation (e.g. with firing rates >40 Hz) quickly slowed their firing (Figure 5B,C). This sensory adaptation was evoked by all odors tested and all concentrations whenever the initial firing rate exceeded ~40 Hz (Figure 5D,E). Faster-firing ORNs underwent greater adaptation (Figure 5E), suggesting ORNs better-tuned for a given odor would adapt more. Thus, we found that each ORN fired at a rate tightly constrained by adaptation and saturation.

To quantify the dynamic range of individual ORNs relative to that of the population, we fit concentration response curves with the Hill equation (Figure 5F,G; Firestein et al., 1993; Wachowiak and Cohen, 2001; Koulakov et al., 2007). In our sample of ORNs and odors we found response thresholds were widely distributed across concentrations spanning about 6 orders of magnitude (C_{10}, Figure 5H). Consistent with this, increasing numbers of ORNs participated in the response as odor concentrations increased (Figure 5F,H). And, most ORNs had Hill coefficients greater than 1 (mean = 1.1269; median = 0.802), corresponding to a dynamic range spanning less than 2 orders of magnitude (Figure 5I,J; Koulakov et al., 2007). The 2 orders of magnitude encoded by individual ORNs corresponded to only about 2/6, or 33% of the dynamic range provided by the whole ORN population. Further, we found that the firing rates in the ORN population fit Gaussian distributions (Figure 5K). As odor concentration increased, the width of the distribution (number of responsive ORNs) broadened but the height of the distribution (firing rate) remained about the same (Figure 5K). These results indicate that, in the moth, the great majority of olfactory dynamic range is encoded as changes in the size of the population of responsive ORNs.

Firing rate adaptation in ORNs determines oscillation frequency

Our analysis of individual ORNs revealed that the frequency transition in LFP oscillations followed a temporal profile closely matching that of the adaptation rate of the most active ORNs (Figure 5L; Figure S6). Yet, experimentally changing the intensity of input to the ORNs (odor concentration) had little if any such effect. To explain these apparently contradictory findings and to understand how oscillation frequency is determined, we incorporated our physiological measurements into a full-scale, map-based model (reduced type, Rulkov et al., 2002; Rulkov et al., 2004; Rulkov and Bazhenov, 2008) of the moth AL (Figure 6A). We simulated input to the AL network as synaptic currents applied to odor- and concentration-specific populations of PNs and LNs (Assisi et al., 2007; see Experimental Procedures). In our model, as *in vivo*, this input caused the population of PNs to spike and to synchronize through feedback inhibition mediated by LNs (Figure 6B). Synchronized spiking in the model AL was manifest as periodic oscillations of the LFP (Figure 6B, top; calculated as the average activity of all PNs).

We had found that the adaptation of ORN firing rates followed a temporal profile matching that of the frequency transition in LFP oscillations (Figure 5L; Figure S6). How does adaptation influence the dynamical properties of the AL network? To simulate activation and adaptation of the odor responses of ORNs, we drove our network model with a rapidly rising and then slowly decaying input (Figure 6B, bottom) with the size of the AL population receiving external stimulation (input "width") held constant. During the simulated odor's onset, the rapid increase in input intensity quickly entrained the network to generate ~40 Hz oscillations (Figures 6B,C). The subsequent decrease in stimulus amplitude initially led to a reduction in the LFP amplitude, signaling a decrease in the synchrony of spiking across the population of responsive PNs. But as the input intensity continued to decrease, synchrony suddenly resumed, although now at ~20 Hz. During this transition the inter-spike interval (ISI) distributions of both PNs and LNs (Figure 6C,D) lengthened. Our intracellular recordings from PNs and LNs had revealed qualitatively similar changes in ISI distribution (Figure S7). In our model, a 40-50% decrease in stimulus intensity caused a frequency shift (Figure 6B) matching what we had observed *in vivo* (Figure 1D,F). This result suggested that a change in stimulus intensity similar to what occurs *in vivo*, and not the size of the responsive ORN population, could explain much of the change in oscillation frequency. Other factors such as the strengths and the time constants of synaptic currents could influence oscillation frequency as well (Figure S8).

We next analyzed the steady-state network dynamics of our model as a function of input intensity. Throughout these stimulations we held constant both the size of the AL population receiving external input and the amplitude of the input; in separate experiments we systematically changed the input amplitude to explore a broad space of parameters. Our model showed that the AL network could generate oscillations with a wide range of frequencies, including 20-40 Hz, depending on the net intensity of its input (Figure 6E, left panel). Further, individual PNs and LNs could change average firing rate as a function of excitatory and inhibitory input intensity (Figure 6E middle and right panels). In our model, inhibitory LNs almost always spiked at the frequency of the LFP oscillations; notably, excitatory PNs could fire faster with either one or two spikes during each oscillatory cycle (Figure 6C,D). These results match those of our intracellular recordings (Figure S7).

How do changes in odor concentration influence the dynamical properties of the AL network? Our model had shown that, for a network with a fixed number of responsive neurons, increasing the amplitude of external stimuli led to a progressive increase in oscillation frequency (Figure 6E). But, our recordings from ORNs had shown that, as the concentration of an odorant increased, more types of receptors began to respond (Figure 5K; see also Stewart et al., 1979; Duchamp-Viret et al., 2000; Wachowiak and Cohen, 2001; Hallem and Carlson, 2006). To simulate this effect of changing odor concentration we varied the proportion of the PN and

LN populations (parameter σ, width of the curve in Figure 7A; compare to Figure 5K) driven by external excitatory input. We found that varying the size of the stimulated neuronal population only slightly varied the frequency of oscillations (Figure 7B-D). When driven by very low odor concentrations ("narrow" input, i.e. σ=0.2), the frequency of LFP oscillations increased slowly upon odor onset (Figure 7C left); several oscillatory cycles were required to engage all the neurons in oscillatory dynamics. Our model suggested that the main effect of varying the size of the responsive neuronal population was to vary the coherence of the moth AL network, but not its frequency.

Our results showed that when sensory input underwent adaptation, two factors changed: 1) active PNs decreased their firing rates; and 2) the size of the active PN population decreased (Figure 6 B,C). To test which factor most directly underlies the oscillator's frequency shift, we provided our model a simplified square input profile rather than a realistic Gaussian input profile; the simplified input drove all stimulated PNs and LNs identically and gave zero input to all non-stimulated PNs and LNs, thus holding the size of the active PN population constant over time even as the input adapted. With this constrained input, adaptation still caused the oscillatory frequency to decrease (Figure S9A). In contrast, decreasing the size of the stimulated AL population (to model a decrease in odor concentration) did not affect oscillation frequency (Figure S9B). Consistent with this result, an even simpler model consisting of only a single PN and a single LN, reciprocally-coupled (Fig 7D), showed that changing the intensity of the input caused a shift in oscillation frequency (Figure 7E). Taken together, these models suggest that input intensity regulates the firing frequency of active PNs, which directly determines the network oscillatory frequency.

A subset of strongly activated PNs regulates oscillatory frequency

To test the robustness of our results and to gain a more intuitive understanding of the mechanism that underlies the oscillatory response transition in the AL, we designed an additional, simplified "firing rate" version of our more realistic map-based model of the AL network (see Experimental Procedures).

To test whether the oscillatory frequency of the AL network is determined by the firing rates of activated PNs, we systematically varied the threshold required to activate PNs, effectively removing weakly-activated ORNs from the network (Figure 8A). Even though this manipulation (like decreasing odor concentration) greatly decreased the size of the active population of neurons and caused the overall input to the network to change dramatically (Figure 8B), the oscillatory frequency remained constant (Figure 8C). Next, we simulated the effect of sensory adaptation by altering the response intensity of the most strongly activated PNs (Figure 8D). This manipulation, which kept the number of active neurons constant but reduced overall input to the network (compare Figure 8B and 8E), greatly altered oscillatory frequency (Figure 8F), consistent with results we obtained with our map-based model and with our physiology experiments.

Further, our simplified rate model showed that adaptation of the ORNs was sufficient to shift the oscillatory frequency of the AL network (Figure 8G-H); a version of the model lacking adaptation showed no shift in frequency (Figure 8I-J). These results, combined with those of our physiological recordings and map-based model show that, for any given odor or concentration, oscillation frequency is controlled by a small subset of ORNs and PNs, those that are most highly responsive.

In summary, our computational models (Figures 6-8) demonstrated that the shifts in LFP frequency we observed *in vivo* during lengthy odor stimulations can be explained by gradual changes in the intensity of output from a stable group of ORNs to the AL. This intensity level is determined mainly by the adaptation and saturation of the peripheral receptor neurons

(ORNs) rather than by the intensity of the environmental stimulus (odor concentration). Our results show that, in the periphery, the great majority of the olfactory system's dynamic range is encoded by the size of the responsive receptor population rather than by its firing rate. Our results also resolve an apparent contradiction, that oscillation frequency follows the intensity of the net receptor output (amplitude of the EAG) but not the concentration of the odor. These findings are summarized in Figure 9.

Discussion

Odor elicited oscillations in the moth

In the moth *Manduca sexta*, our intracellular recordings from PNs, LNs and KCs together with recordings of the LFP from the MB and AL (Figures 1-3) revealed that moths employ essentially the same neural mechanism as that characterized in the locust and *Drosophila*: oscillations are generated in the AL via $GABA_A$-type inhibition (Figure S3), build up gradually over repeated odor presentations (Figure S1; Stopfer and Laurent, 1999) and influence the fine spike timing of downstream KCs (Laurent, 2002;Perez-Orive et al., 2002,Assisi et al., 2007;Tanaka et al., 2009).

This result contradicts several earlier reports. Previously, in the moth, pulses of pheromone were found to induce highly localized LFP oscillations only within the AL, with spikes in pheromone-sensitive PNs phase-locked to the AL-LFP oscillations (Heinbockel et al., 1998). However, such stimuli were described as never producing coherent LFP oscillations between the MB and the AL (Christensen et al., 2003). Further, in a multi-unit recording experiment (Christensen et al., 2000) and a double intracellular recording experiment (Lei et al., 2002), cross-correlation analyses detected no sustained oscillatory synchrony between pairs of PNs but rather only brief, stimulus-locked, non-oscillatory synchrony. These observations led to the proposal that, in *Manduca*, only transient, non-oscillatory synchronous activity among PNs supports odor coding, likely by promoting coincidence detection by downstream elements (Lei et al., 2002). Our experiments employed general, non-pheromonal odors, such as host plant volatiles and common food blends at a wide range of concentrations. The differences in our results from those reported earlier probably arise both from our focus on the general olfactory system rather than the pheromone system, and from differences in recording techniques (likely the electrode's shape and internal solution; see Experimental Procedures). The moth pheromone system, which, within the AL, consists of three specialized glomeruli anatomically separate from the ~60 glomeruli of the general odor system (Rospars and Hildebrand, 1992), may not provide an ideal model for all aspects of general olfaction.

Indeed, our results show that, to a remarkable extent, odor coding mechanisms in *Manduca* are similar to those of other species, including *Drosophila* (Tanaka et al., 2009), honeybee (Stopfer et al., 1997), and locust (Laurent and Naraghi, 1994; MacLeod and Laurent, 1996; Perez-Orive et al., 2002). This was perhaps unexpected because these species differ in details of olfactory anatomy and physiology. The ~60 ordinary glomeruli in the AL of *Manduca* compare roughly in number to many other insects (Anton and Homberg, 1999), and the great majority of its PNs are uniglomerular (Homberg et al., 1989). By contrast, in the locust, the AL is organized into ~1000 microglomeruli (Ernst et al., 1977) which are heavily interconnected through multiglomerular PNs (each visiting 12-24 glomeruli), and extensively arborized LNs (MacLeod and Laurent, 1996). In *Manduca* LNs generate full-size sodium spikes. But in the locust, LNs produce graded calcium potentials rather than all-or-none spikes. Because of its microglomerular structure and extensive multiglomerular connectivity, the locust olfactory system has sometimes been described as atypical (Hansson and Anton, 2000). Nevertheless, our results strongly suggest that, despite substantial differences in anatomical detail, the olfactory systems of these species function in a remarkably similar fashion.

Despite the striking similarities in odor coding mechanisms in locust and moth, we found small differences. The oscillatory phase relationship between spikes in PNs and LNs is slightly different in the two animals, possibly because of differences in the timing of spikes in LNs. In the locust the population of PNs spikes with the greatest synchrony upon odor onset (Mazor and Laurent, 2005) probably because the strong, non-adapted input can activate many LNs which coordinate the spike timings of PNs (Assisi et al., 2007). In the moth, we found that odor inputs were strongest at the odor onset as well (Figure 5C,D). However, both across LNs and PNs, synchrony increased gradually over the course of a response (Figure S4). This is probably because, in the moth, oscillation frequency at the odor's onset shifted too quickly to permit full entrainment of the oscillatory network. Indeed, frequency shifts we observed in the moth over the course of a stimulus were typically greater than those in the locust (Figure S2; see also Perez-Orive, 2004). Our simplified rate model suggests this difference could be explained by greater net inhibition in the locust: we found that if we slightly increased the strength of inhibition in our simplified model of the moth AL, the model then produced frequency shifts similar to those observed in the locust (Figure S10). We speculate that, compared to the moth, the balance of net excitation and inhibition is slightly shifted toward stronger inhibition in locust.

Adaptation and saturation of ORN firing rate determine the oscillation frequency

Our recordings revealed that additional ORNs were recruited into the responsive population as odor concentration increased (Figure 5), a result consistent with a fundamental property of receptors: they become less selective as the concentrations of ligands increase. Yet, we found the range of response intensity of these ORNs was sharply constrained. Long odor pulses caused the most highly responsive ORNs to rapidly adapt their firing rates, with a time course similar to that of the shift in oscillation frequency (Figure 5L). Further, the firing rates of the most precisely tuned ORNs saturated when stimulated by low to moderate odor concentrations (Figure 5C-F).

Our electrophysiological and computational approaches allowed us to compare the relative contributions of the size of the responsive population and its response intensity. We found that in the periphery, coding of odor concentration was heavily dominated by the size of the set of responsive ORNs rather than by the intensity of the response of the ORNs. At low odor concentrations, only those receptors most precisely tuned to the odor responded; as the concentration increased, the precisely-tuned ORNs continued to fire, but quickly adapted and saturated, and thus displayed strictly constrained increases in response intensity. However, additional, less well tuned ORNs began to participate in the response, thus encoding the concentration of the odor.

Several lines of evidence indicate that information about odors is encoded by a population of ORNs in a combinatorial fashion (Buck, 1996). A recent comprehensive study of all the receptor types on the *Drosophila* antenna (Hallem and Carlson, 2006) showed that the firing rates of ORNs often saturated at moderate concentration, that some ORNs decreased their firing rates at extremely high concentrations, and that, at high concentrations, individual ORNs tended to respond broadly to many odors. Studies using 2-deoxyglucose labeling, c-fos and calcium images have shown that the spatial pattern of glomerular activation can expand as odor concentration increases (for review see Buck, 1996). Further, several studies suggest that ORNs can respond within a narrow dynamic range (Firestein et al., 1993; Stewart et al., 1979; Koulakov et al., 2007). Indeed, a theoretical study of the locust olfactory system predicted that an intensity coding scheme like that shown here could explain the invariant frequency of odor-evoked oscillations over a wide range of stimulus intensity (Asissi et al., 2007). These results are consistent with our quantitative finding that odor intensity is encoded mainly by the size of active ORN population rather than by firing rates.

We incorporated our findings in the moth into two types of computational models to determine how sensory input to an oscillatory circuit influences its frequency. Our models robustly mimicked the frequency transition we observed between fast and slow oscillatory states as input intensity gradually decreased (Figures 6-8, S10). Further, our models demonstrated that recruiting additional, but less well-tuned, ORNs could simulate responses to higher odor concentrations while causing only minimal changes in oscillation frequency (Figures 7,8), similar to what we observed *in vivo* (Figures 4-5). Our models also demonstrated how oscillation frequency can shift between fast and slow states (Figures 6,8), depending mainly upon the varying output intensity of rapidly saturating and adapting receptors, rather than upon odor concentration.

In agreement with earlier work in locust (Stopfer et al., 2003) our results show that increases in odor concentration led to large increases in the coherence of the odor-triggered oscillatory synchrony of PNs (Figure 4C). This large increase in coherence was accompanied by only small changes in the frequency of oscillation (Figure 4D), and was caused mainly by increasing the size of the activated ORN population. Our results show that, in the moth AL, the coherence and the firing rate of the PN ensemble are determined independently (for a discussion of theory see Salinas and Sejnowski, 2001). This independence enables an efficient strategy for dynamically matching the firing properties of PNs to the coincidence detection-based decoding properties of KCs (Perez-Orive et al., 2002; 2004).

What are the implications of this transition during an odor response? A comparison of the jitter in spike timing relative to the LFP before and after the frequency transition revealed an increase in spike time precision in LNs, PNs and KCs (Figure S4). Because little is known about how the output of KCs is decoded by cells that follow them, potential benefits of this increase in spike precision are not immediately apparent. One possibility is that the increase in the synchrony of input to the KCs might help sustain highly specific firing in these cells even though the output of PNs decreases when ORNs adapt.

A similar frequency transition from gamma to beta oscillations has been noted in the rat olfactory bulb (Neville and Haberly, 2003), but the mechanism underlying the transition is quite different from that shown here. In the rat, oscillations of different frequency are generated by different neural circuits: odor-evoked gamma oscillations in the olfactory bulb arise locally, but beta oscillations require the participation of the olfactory cortex (Neville and Haberly, 2003).

It is well established that shifts in the balance of excitation and inhibition (Brunel and Wang, 2003) or changes in excitatory drive (Whittington et al., 1995; Traub et al., 1996) can influence the oscillation frequency of a neural network. However, sensory systems characterized *in vivo* often generate oscillations of invariant frequency when driven by a wide range of stimulus intensities (Bringuier et al., 1997; Stopfer et al., 2003; Schadow et al., 2007). Our results suggest the extent to which oscillation frequency is sensitive to stimulus intensity depends at least in part on the properties (such as adaptation and saturation) of the neurons that provide inputs to the oscillatory network. In the retina, for example, some classes of ganglion cells have been shown to increase their firing rates as the velocity of a moving visual stimulus increases (Cleland and Harding, 1983); concomitantly, the frequency of gamma oscillations in the visual cortex monotonically increases (Gray and Prisco, 1997). On the other hand, in cortical areas responsive to the orientation or direction of a visual stimulus, oscillation frequency remains constant (Gray and Singer, 1989), likely because changing these stimuli only changes the population of active cells. That many primary sensory neurons display tuning, saturation and adaptation characteristics may help explain why invariant oscillation frequency is often observed in sensory systems (Bringuier et al., 1997; Stopfer et al., 2003; Schadow et al., 2007).

Oscillatory dynamics and fast-firing principal neurons

Fast 20-60 Hz synchronized oscillations are common in neuronal circuits. In one form of gamma oscillations (Interneuron Network Gamma, ING) a network of mutually inhibiting interneurons exclusively establishes the rhythm; pyramidal cells are simply entrained to it, and their low firing rates have little or no effect on network oscillations (Whittington et al, 2000; Wang and Buzsaki 1996). But in our models oscillations failed when synaptic input from PNs to LNs was blocked (data not shown). This suggests odor triggered oscillations in the moth AL are not entirely mediated by an ING-type inhibitory network but rather require the active participation of excitatory PNs to drive LNs (indeed, we observed that moth PNs fired slightly before LNs; Figure 2C) which in turn synchronized PNs through feedback inhibition. In this respect, odor triggered oscillations in the moth AL are similar to the persistent/transient forms of gamma oscillations (Pyramidal-Interneuron Network Gamma, PING) in the vertebrate cortex and hippocampus.

Our intracellular recordings from the AL network revealed, however, an unusual situation: most active PNs fired faster than the oscillation frequency (Figure S7). More typically, as in the case of transient gamma oscillations induced by tetanic stimulation of the hippocampus (Traub et al., 1996; Whittington et al., 1997), fast spiking interneurons and pyramidal cells both fire at the oscillation frequency. Also, during persistent gamma activity in CA3 (Fisahn et al., 1998) and neocortex (Buhl et al., 1998), interneurons fire on every cycle or every other cycle; pyramidal cells fire at much lower rates. Notably, our model demonstrated that stable oscillations can nevertheless emerge from a network with fast-firing PNs (Fig 6B-D), a condition thought to be unstable since excessive excitatory feedback from PNs to LNs could potentially disrupt the rhythmic LN network.

The stability of the regime we observed in the moth could be explained by the combination of high-rate excitation and relatively low-efficiency GABA$_A$-mediated inhibition revealed by our recordings and our models. The overall weak inhibition we found in the moth AL (Figure S10) could also explain the relatively weak dependency of the network oscillation frequency upon the decay time constant of inhibition. Indeed, if fast, GABAergic inhibition were strong enough to prevent excitatory cells from firing, oscillatory frequency would depend strongly on the time constant of inhibition (Whittington et al., 1995; Buzsáuki and Chrobak, 1995; Brunel and Wang, 2003; Bazhenov et al., 2008), something we did not observe here (Figure S8B,C). In moth, the net impact of inhibition seems restricted to influencing the timing of spikes in excitatory neurons, thus enabling periodic network rhythms. However, this inhibition appears too weak to prevent excitatory cells from firing, enabling them to maintain firing frequencies that exceed the network oscillation frequency. The oscillatory regime revealed here may be common, particularly in insects; unlike pyramidal cells, PNs in the AL of honeybee (Stopfer et al., 1997), locust (Stopfer et al., 2003), and *Drosophila* (Olsen et al., 2007) can respond to stimuli with high firing rates.

Experimental Procedures

Olfactory stimulation

Odor stimulation was modified from Brown et al (2005). Briefly, the odorized headspace in 60-ml glass bottles above mineral oil-diluted odorant solution (10 mL) was pushed by a controlled volume of humidified air (0.1 L/min) into an activated carbon-filtered, humidified air stream (0.75 L/min) flowing continuously across the antenna. The longest stimulus we used (4-s) would deplete only about 13% of the vapor in the headspace, making it likely that each odor pulse varied little in concentration throughout each stimulus. All chemicals were purchased from Sigma-Aldrich (St. Louis, MO) unless otherwise noted. Odorants were benzylalcohol, benzaldehyde, (+)-β-citronellene (Fluka Chemika, Buchs, Switzerland),

cyclohexanone, geraniol, hexanol, cis-3-hexenyl acetate, (±)linalool (Aldrich Chemical Company Inc, Milwaukee, WI), methyl salicylate, methyl jasmonate, 1-octanol (Fluka Chemika, Buchs, Switzerland), trans-2-hexenal, trans-2-hexen-1-ol, oil extracts (strawberry, cinnamon, peach, lime, jasmine, Balducci's, Bethesda, MD), thyme (Thyme Red, Saidel Inc., Renton, WA), and wintergreen (Wagner's). Odorant solutions were diluted (vol/vol) to 1% in mineral oil (J.T. Baker, Phillipsburg, NJ) unless otherwise noted.

Electrophysiology

Physiological data were obtained from 145 adult moths (*Manduca sexta*) of both sexes reared from eggs (purchased from the NCSU Insectary, Raleigh, NC) in our laboratory on an artificial diet (Bell and Joachim, 1976), under a long-day photoperiod at 26 °C, and at more than 70% relative humidity. Adults 1 d post-eclosion or older were dissected as described previously (Ito et al., 2008). The head capsule was superfused with moth physiological saline (Christensen and Hildebrand, 1987) at room temperature.

EAGs were recorded using Ag/AgCl wire (127 μm o.d.) inserted into the distal tip of the antenna; the reference wire was inserted into the contralateral compound eye. Signals were amplified with a DC amplifier (Model 440; BrownLee Precision, San Jose, CA).

LFPs were recorded using saline-filled glass micropipettes with a long-shank (o.d. ~3 μm, 4-10 MΩ), amplified and low-pass filtered (>100 Hz) by a DC amplifier (Brown-Lee Model 440). The long-shank could be inserted deep into the calyx of the MB where axons of PNs and the dendrites of followers Kenyon cells make synaptic contacts. This technique allowed us to record LFP oscillations more robust than those we could detect by the method we use in locust (a blunt ended glass electrode with a short shank placed on the cell body layer of the MB; see Brown et al., 2005).

Extracellular recordings of ORNs from were made from sensilla in either isolated antennae cut at their bases or intact antennae of restrained animals (both methods yielded identical results). The antenna was stabilized with epoxy glue carefully applied to leave the leading surface (where sensilla are located) accessible. An electrochemically-sharpened tungsten wire was inserted into the sensillar base under a stereomicroscope (Leica MZ7.5). For isolated antenna preparations, Ag/AgCl wires were placed in the cut ends. The proximal cut end was immersed in a drop of saline or sensillum lymph (Kaissling, 1995) which was covered with wax to prevent evaporation. For intact antenna preparations, Ag/AgCl wires were placed in the distal end of the antenna and the contralateral compound eye. Signals were amplified by a differential amplifier (P55, GRASS Instrument; Telefactor, W. Warwick, RI) and sampled at 15 kHz (LabView software, PCI-MIO-16E-4 DAQ cards, National Instruments).

Intracellular recordings, subsequent fluorescent dye injection, histological steps and confocal imaging were made using sharp glass micropipettes as described previously (Ito et al., 2008).

Full scale AL network model

The AL model included 820 PNs and 360 LNs (Homberg et al., 1989) simulated using a reduced neuron model written in the form of difference equations (map; Rulkov 2002; Rulkov et al. 2004; Bazhenov et al. 2005; Rulkov and Bazhenov, 2008). The time evolution of membrane

voltage V_n was described as nonlinear map $V_{n+1}=f_\alpha\left(V_n, I_n+\beta^e I_n^{ext}\right)$, where I_n is a slow dynamical variable describing the effects of slow conductances, f_α is nonlinear function and n is a discrete time step (~0.5 ms). The model's properties and parameters are shown in Figure S11. This model, despite its low intrinsic dimensionality, produces a rich repertoire of dynamics and is able to mimic the dynamics of Hodgkin-Huxley type neurons both at the single cell level

and in the context of network dynamics (Rulkov et al, 2004; Bazhenov et al, 2005; Rulkov and Bazhenov, 2008).

For synaptic connections, we used conventional first order kinetic models of fast synaptic conductances (Rulkov et al. 2004; Bazhenov et al. 2005) (see Fig. S11). All intrinsic connections (LN-LN, LN->PN, PN->LN) were random with 0.5 probabilities. Maximal conductances (in dimensionless units; see Rulkov et al., 2004) denoting the total excitation and inhibition received by a given cell were set in most of the simulations to G_{ACh}(PN-LN) = 0.00015, G_{GABA}(LN-PN) = 0.00035, G_{GABA}(LN-LN) = 0.00015.

The intensity (amplitude) of external (to mimic odor) stimuli to PNs and LNs followed a Gaussian distribution truncated at 0.1 to avoid stimulating all PNs (see Figure 7A). Which PNs and LNs received input with a particular intensity was determined randomly. The proportion of LNs receiving non-zero input was approximately one third that of PNs receiving non-zero input. For simplicity, we assumed that all ORNs (not only the best tuned ones) undergo sensory adaptation. To mimic data obtained *in vivo*, the temporal variation of the stimulus was approximated by the experimentally-measured function shown in Figure 5L.

Simplified firing rate model

This simplified model contained 80 PNs and 30 LNs; qualitatively similar results were obtained with a version of the model containing 800 PNs and 300 LNs. The dynamics of each neuron in the network was modeled as a difference equation:

$$\frac{dv_j}{dt} = -\frac{v_j(t)}{\tau} + \sum_{k=1}^{N} W_{kj}\varphi(v_k(t)) + I_j$$

where v_k is the out firing rate of neuron k, τ is the membrane time constant of neuron ($\tau = 10$ ms) and φ is a non-linear logistic function ($\varphi(x) = [1 + \exp(-a_1 \cdot (x - a_2))]^{-1}$; a1 = 10, a2 = 0.6). I_j is the input from *ORN* type j to PN_j. LNs did not receive direct input from ORNs. The connectivity matrix W included 50% connection probability: PN->LN ($W_{PN\_LN} = 0.125$) and LN->PN ($W_{LN\_PN} = -0.2$). No PN->PN or LN->LN connections were included. The integration step size (dt) was set to 1 ms. The model LFP was computed by filtering summed PN activity (V). Since the number of PNs was reduced in this model, LFP traces shown appear noisy.

Each ORN response was modeled after our physiological recordings. The initial response from baseline to peak amplitude followed $t \cdot \exp(-t/\tau_{rise})$. Subsequently, ORN responses were reduced to reach an adapted state set at 60% of the peak amplitude following $\exp(-t/\tau_{adapt})$. Finally, after the odorant was removed, ORN responses returned back to baseline following $\exp(-t/\tau_{fall})$. τ_{rise}, τ_{adapt}, τ_{fall} for all 80 ORNs were set to 100 ms, 200 ms and 250 ms, respectively. For any odor 40% of PNs received non-zero ORN input. Peak ORN response amplitude was uniformly, randomly distributed between [0,1]. Model EAG responses (Figure 8G,I) were computed by summing individual ORN firing-rate responses.

Data analysis

All analyses except for spike sorting were performed using custom programs in MATLAB (MathWorks Inc., Natick, MA). For experiments examining the effect of odor pulse duration on oscillation frequency, 10 pre-trials (4 s) were first delivered to elicit short-term "fast learning" response plasticity (Stopfer and Laurent, 1999), and then 100, 250, 500, 750, 1000, 1500 ms duration pulses were examined in a pseudorandom sequence; this set was repeated 3 times in each animal. Spectrograms (500 ms sliding Hamming window with 90% overlap)

were normalized by the maximum value in the last pre-trial. Results from 18 trials each from 3 animals of either sex (each animal tested with 2 odors) were averaged.

We used a magnitude squared coherence measure in Figure 1F to compare LFPs recorded in the AL and the MB; this approach allowed us to minimize the effect of small variations in phase we found in AL recordings caused by differences in electrode placement. We calculated the magnitude squared coherence using an overlapping sliding Hamming window (0.25 s with 80% overlap) for fast (0.25-1 s) and slow (1-4 s) oscillations. For Figure 3B, which did not require phase comparisons across brain structures, we used the more standard cross-correlation measure.

We computed the phase of each spike relative to MB oscillations for fast (0.3-0.8 s) and slow (0.8-4 s) oscillations as described elsewhere (Mazor and Laurent, 2005) but modified as follows. LFP signals were acquired through an analog low-pass filter (>100 Hz) of a DC amplifier (BrownLee Model 440), which imposed a 7 ms delay, which we compensated for in MATLAB. For the phase analysis, LFP signals were then digitally filtered (5-55 Hz, Butterworth; zero phase distortion by filtfilt command in MATLAB).

We measured the frequencies of LFP oscillations evoked by different concentrations of three odors, each tested in blocks of 10 trials that were given in a randomized order. Power spectra were computed using the time series in the first 0.5 s of odor responses as well as in the 1 s before the odor responses (basal activity) and then averaged across 10 trials. The oscillation frequency was determined as the frequency with the maximum power in 14-54 Hz band in the average power spectrum.

Spike sorting of sensillum recordings was performed offline using Spike-o-Matic software (Pouzat et al., 2002) implemented in Igor Pro (Wavemetrics, Lake Oswego, OR). In ORNs, spike amplitude can change somewhat as ORNs adapt to odors; to accommodate small changes in spike amplitude we allowed each cell cluster to include events with varying amplitudes as long as different sorted clusters remained well-separated (by at least 5 times noise standard deviation), and, within a cluster, an appropriate inter-spike interval distribution was maintained throughout an experiment. For the population firing rate analysis shown in Figure 5D,E, in addition to well-sorted units, we included unsorted data as multiunit activity from a single sensillum. All other panels in Figure 5 include only well-sorted ORNs.

To fit the concentration responses of ORNs, we first counted the number of spikes in the first 1 s of odor response (same analysis bin as F1 in Figure 5D) and averaged over 10 trials for each concentration. Similarly, the baseline activity was measured from the 2 s just before the odor onset. ORN-odor combinations not showing odor-elicited changes in spiking (<5 spikes/ response) were not included in this analysis.

Supplementary Material

Refer to Web version on PubMed Central for supplementary material.

Acknowledgments

References

Adrian ED. Olfactory reactions in the brain of the hedgehog. J. Physiol 1942;100:459–473. [PubMed: 16991539]

Anton, S.; Homberg, U. Antennal lobe structure. In: Hansson, BS., editor. Insect Olfaction. Springer-Verlag; Berlin: 1999. p. 101

Assisi C, Stopfer M, Laurent G, Bazhenov M. Adaptive regulation of sparseness by feedforward inhibition. Nat. Neurosci 2007;10:1176–1184. [PubMed: 17660812]

Bazhenov M, Rulkov NF, Fellous J-M, Timofeev I. Role of network dynamics in shaping spike timing reliability. Phys. Rev. E. Stat. Nonlin. Soft Matter Phys 2005;72:041903. [PubMed: 16383416]

Bazhenov M, Rulkov NF, Timofeev I. Effect of synaptic connectivity on long-range synchronization of fast cortical oscillations. J. Neurophysiol 2008;100:1562–1575. [PubMed: 18632897]

Bell RA, Joachim FA. Techniques for rearing laboratory colonies of tobacco hornworms and pink bollworms lepidoptera-sphingidae-gelechiidae. Ann. Entomol. Soc. Am 1976;69:365–373.

Bressler SL, Freeman WJ. Frequency analysis of olfactory system EEG in cat, rabbit, and rat. Electroencephalogr. Clin. Neurophysiol 1980;50:19–24. [PubMed: 6159187]

Bringuier V, Frégnac Y, Baranyi A, Debanne D, Shulz DE. Synaptic origin and stimulus dependency of neuronal oscillatory activity in the primary visual cortex of the cat. J. Physiol 1997;500(Pt 3):751–774. [PubMed: 9161989]

Brown SL, Joseph J, Stopfer M. Encoding a temporally structured stimulus with a temporally structured neural representation. Nat. Neurosci 2005;8:1568–1576. [PubMed: 16222230]

Brunel N, Wang X-J. What determines the frequency of fast network oscillations with irregular neural discharges? I. Synaptic dynamics and excitation-inhibition balance. J. Neurophysiol 2003;90:415–430. [PubMed: 12611969]

Buck LB. Information coding in the vertebrate olfactory system. Annu. Rev. Neurosci 1996;19:517–544. [PubMed: 8833453]

Buhl EH, Tamás G, Fisahn A. Cholinergic activation and tonic excitation induce persistent gamma oscillations in mouse somatosensory cortex in vitro. J. Physiol 1998;513:117–126. [PubMed: 9782163]

Buzsáki G, Chrobak JJ. Temporal structure in spatially organized neuronal ensembles: a role for interneuronal networks. Curr. Opin. Neurobiol 1995;5:504–510. [PubMed: 7488853]

Christensen TA, Hildebrand JG. Male-specific, sex pheromone-selective projection neurons in the antennal lobes of the moth Manduca sexta. J. Comp. Physiol. [A] 1987;160:553–569.

Christensen TA, Lei H, Hildebrand JG. Coordination of central odor representations through transient, non-oscillatory synchronization of glomerular output neurons. Proc. Natl. Acad. Sci. U. S. A 2003;100:11076–11081. [PubMed: 12960372]

Christensen TA, Pawlowski VM, Lei H, Hildebrand JG. Multi-unit recordings reveal context-dependent modulation of synchrony in odor-specific neural ensembles. Nat. Neurosci 2000;3:927–931. [PubMed: 10966624]

Cleland BG, Harding TH. Response to the velocity of moving visual stimuli of the brisk classes of ganglion cells in the cat retina. J. Physiol 1983;345:47–63. [PubMed: 6663509]

Duchamp-Viret P, Duchamp A, Chaput MA. Peripheral odor coding in the rat and frog: quality and intensity specification. J. Neurosci 2000;20:2383–2390. [PubMed: 10704512]

Ernst KD, Boeckh J, Boeckh V. A neuroanatomical study on the organization of the central antennal pathways in insects. Cell Tissue Res 1977;176:285–306. [PubMed: 832298]

Firestein S, Picco C, Menini A. The relation between stimulus and response in olfactory receptor cells of the tiger salamander. J. Physiol 1993;468:1–10. [PubMed: 8254501]

Fisahn A, Pike FG, Buhl EH, Paulsen O. Cholinergic induction of network oscillations at 40 Hz in the hippocampus in vitro. Nature 1998;394:186–189. [PubMed: 9671302]

Galambos R, Makeig S, Talmachoff PJ. A 40-Hz auditory potential recorded from the human scalp. Proc. Natl. Acad. Sci. U. S. A 1981;78:2643–2647. [PubMed: 6941317]

Gray CM, König P, Engel AK, Singer W. Oscillatory responses in cat visual cortex exhibit inter-columnar synchronization which reflects global stimulus properties. Nature 1989;338:334–337. [PubMed: 2922061]

Gray CM, Prisco GVD. Stimulus-dependent neuronal oscillations and local synchronization in striate cortex of the alert cat. J. Neurosci 1997;17:3239–3253. [PubMed: 9096157]

Gray CM, Singer W. Stimulus-specific neuronal oscillations in orientation columns of cat visual cortex. Proc. Natl. Acad. Sci. U. S. A 1989;86:1698–1702. [PubMed: 2922407]

Hallem EA, Carlson JR. Coding of odors by a receptor repertoire. Cell 2006;125:143–160. [PubMed: 16615896]

Hansson BS, Anton S. Function and morphology of the antennal lobe: new developments. Annu. Rev. Entomol 2000;45:203–231. [PubMed: 10761576]

Heinbockel T, Kloppenburg P, Hildebrand JG. Pheromone-evoked potentials and oscillations in the antennal lobes of the sphinx moth *Manduca sexta*. J. Comp. Physiol. [A] 1998;182:703–714.

Homberg U, Christensen TA, Hildebrand JG. Structure and function of the deutocerebrum in insects. Annu. Rev. Entomol 1989;34:477–501. [PubMed: 2648971]

Ito I, Ong RC, Raman B, Stopfer M. Sparse odor representation and olfactory learning. Nat. Neurosci 2008;11:1177–1184. [PubMed: 18794840]

Kaissling, K. Single unit and electroantennogram recordings in insect olfactory organs. In: Spielman, A.; Brand, J., editors. Experimental cell biology of taste and olfaction: current techniques and protocols. CRC press; Boca Raton, FL: 1995. p. 367-377.

Kaissling KE, Strausfeld CZ, Rumbo ER. Adaptation processes in insect olfactory receptors. Mechanisms and behavioral significance. Ann. N. Y. Acad. Sci 1987;510:104–112. [PubMed: 3324874]

Koulakov A, Gelperin A, Rinberg D. Olfactory coding with all-or-nothing glomeruli. J. Neurophysiol 2007;98:3134–3142. [PubMed: 17855585]

Laurent G. Olfactory network dynamics and the coding of multidimensional signals. Nat. Rev. Neurosci 2002;3:884–895. [PubMed: 12415296]

Laurent G, Davidowitz H. Encoding of olfactory information with oscillating neural assemblies. Science 1994;265:1872–1875. [PubMed: 17797226]

Laurent G, Naraghi M. Odorant-induced oscillations in the mushroom bodies of the locust. J. Neurosci 1994;14:2993–3004. [PubMed: 8182454]

Lei H, Christensen TA, Hildebrand JG. Local inhibition modulates odor-evoked synchronization of glomerulus-specific output neurons. Nat. Neurosci 2002;5:557–565. [PubMed: 12006983]

MacLeod K, Laurent G. Distinct mechanisms for synchronization and temporal patterning of odor-encoding neural assemblies. Science 1996;274:976–979. [PubMed: 8875938]

Mazor O, Laurent G. Transient dynamics versus fixed points in odor representations by locust antennal lobe projection neurons. Neuron 2005;48:661–673. [PubMed: 16301181]

Neville KR, Haberly LB. Beta and gamma oscillations in the olfactory system of the urethane-anesthetized rat. J. Neurophysiol 2003;90:3921–3930. [PubMed: 12917385]

Olsen SR, Bhandawat V, Wilson RI. Excitatory Interactions between Olfactory Processing Channels in the Drosophila Antennal Lobe. Neuron 2007;54:89–103. [PubMed: 17408580]

Perez-Orive, J. Ph.D thesis. California Institute of Technology; Pasadena, California: 2004. Neural oscillations and the decoding of sensory information.

Perez-Orive J, Bazhenov M, Laurent G. Intrinsic and circuit properties favor coincidence detection for decoding oscillatory input. J. Neurosci 2004;24:6037–6047. [PubMed: 15229251]

Perez-Orive J, Mazor O, Turner GC, Cassenaer S, Wilson RI, Laurent G. Oscillations and sparsening of odor representations in the mushroom body. Science 2002;297:359–365. [PubMed: 12130775]

Pouzat C, Mazor O, Laurent G. Using noise signature to optimize spike-sorting and to assess neuronal classification quality. J. Neurosci. Methods 2002;122:43–57. [PubMed: 12535763]

Rospars JP, Hildebrand JG. Anatomical identification of glomeruli in the antennal lobes of the male sphinx moth *Manduca sexta*. Cell Tissue Res 1992;270:205–227. [PubMed: 1451169]

Rulkov NF. Modeling of spiking-bursting neural behavior using two-dimensional map. Phys. Rev. E. Stat. Nonlin. Soft Matter Phys 2002;65:041922. [PubMed: 12005888]

Rulkov NF, Bazhenov M. Oscillations and synchrony in large-scale cortical network models. J. Biol. Phys 2008;34:279–299. [PubMed: 19669478]

Rulkov NF, Timofeev I, Bazhenov M. Oscillations in large-scale cortical networks: map-based model. J. Comput. Neurosci 2004;17:203–223. [PubMed: 15306740]

Salinas E, Sejnowski TJ. Correlated neuronal activity and the flow of neural information. Nat. Rev. Neurosci 2001;2:539–550. [PubMed: 11483997]

Schadow J, Lenz D, Thaerig S, Busch NA, Fründ I, Herrmann CS. Stimulus intensity affects early sensory processing: sound intensity modulates auditory evoked gamma-band activity in human EEG. Int. J. Psychophysiol 2007;65:152–161. [PubMed: 17531341]

Stewart WB, Kauer JS, Shepherd GM. Functional organization of rat olfactory bulb analysed by the 2-deoxyglucose method. J. Comp. Neurol 1979;185:715–734. [PubMed: 447878]

Stopfer M, Bhagavan S, Smith BH, Laurent G. Impaired odour discrimination on desynchronization of odour-encoding neural assemblies. Nature 1997;390:70–74. [PubMed: 9363891]

Stopfer M, Jayaraman V, Laurent G. Intensity versus identity coding in an olfactory system. Neuron 2003;39:991–1004. [PubMed: 12971898]

Stopfer M, Laurent G. Short-term memory in olfactory network dynamics. Nature 1999;402:664–668. [PubMed: 10604472]

Tanaka NK, Ito K, Stopfer M. Odor-evoked neural oscillations in *Drosophila* are mediated by widely branching interneurons. J. Neurosci 2009;29(26):8595–8603. [PubMed: 19571150]

Traub RD, Whittington MA, Colling SB, Buzsáki G, Jefferys JG. Analysis of gamma rhythms in the rat hippocampus in vitro and in vivo. J. Physiol 1996;493(Pt 2):471–484. [PubMed: 8782110]

Wachowiak M, Cohen LB. Representation of odorants by receptor neuron input to the mouse olfactory bulb. Neuron 2001;32:723–735. [PubMed: 11719211]

Waldrop B, Christensen TA, Hildebrand JG. GABA-mediated synaptic inhibition of projection neurons in the antennal lobes of the sphinx moth, *Manduca sexta*. J. Comp. Physiol. [A] 1987;161:23–32.

Wang XJ, Buzsáki G. Gamma oscillation by synaptic inhibition in a hippocampal interneuronal network model. J. Neurosci 1996;16:6402–6413. [PubMed: 8815919]

Whittington MA, Stanford IM, Colling SB, Jefferys JG, Traub RD. Spatiotemporal patterns of gamma frequency oscillations tetanically induced in the rat hippocampal slice. J. Physiol 1997;502(Pt 3): 591–607. [PubMed: 9279811]

Whittington MA, Traub RD, Jefferys JG. Synchronized oscillations in interneuron networks driven by metabotropic glutamate receptor activation. Nature 1995;373:612–615. [PubMed: 7854418]

Whittington MA, Traub RD, Kopell N, Ermentrout B, Buhl EH. Inhibition-based rhythms: experimental and mathematical observations on network dynamics. Int. J. Psychophysiol 2000;38:315–336. [PubMed: 11102670]
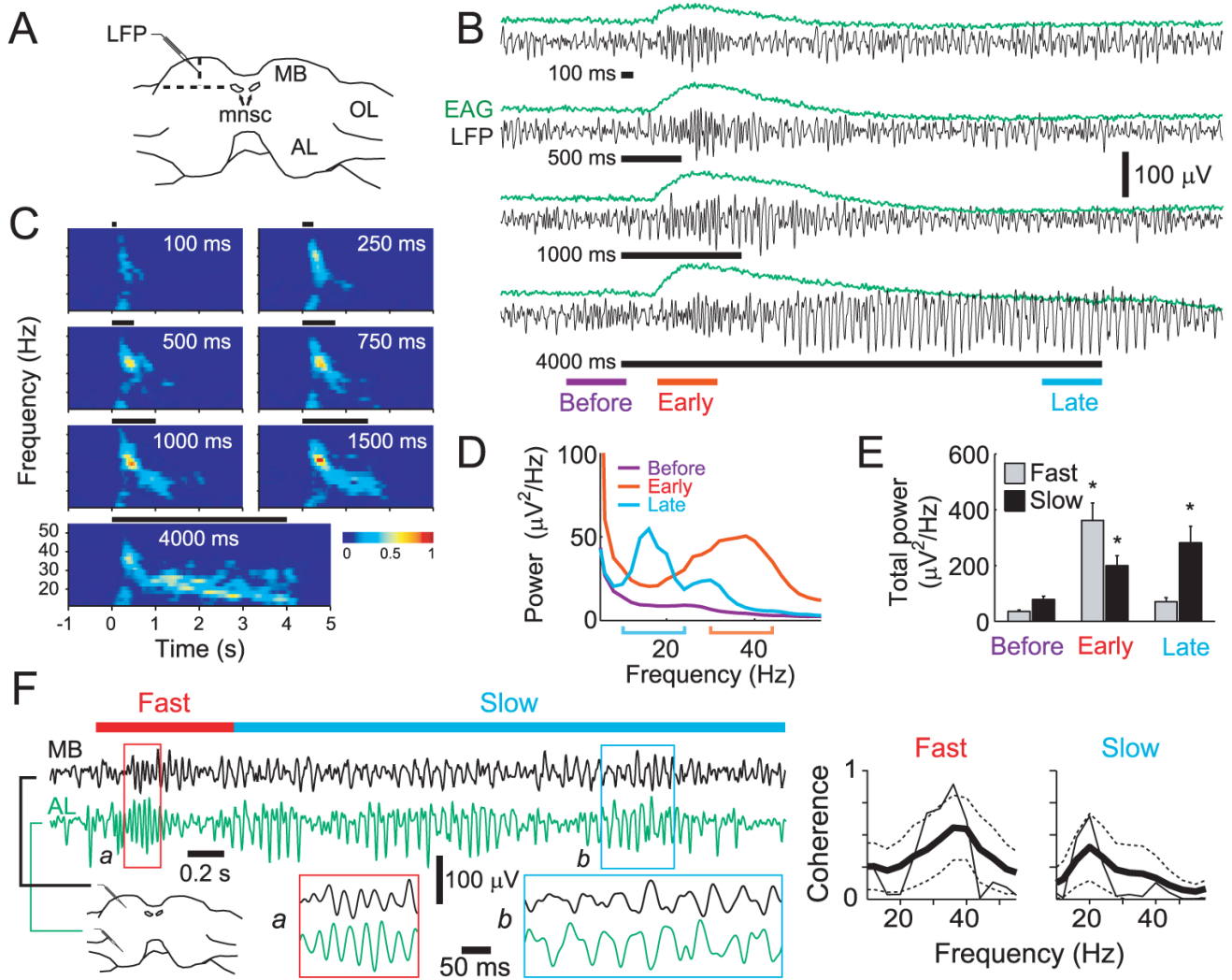
Figure 1. Odors evoked LFP oscillations in the moth MB and AL

(A) Recording site for LFP: center of the calyx in the MB. MB, mushroom body; mnsc, medial neurosecretory cells; OL, optic lobe; AL, antennal lobe.

(B) LFP oscillations (black traces) with simultaneously-recorded electroantennogram (EAG, green traces) evoked by different pulse durations of 1% benzyl alcohol, a plant volatile. Black horizontal bars: odor pulses. Color bars: time windows (500 ms) used to calculate the power spectra in [D].

(C) Brief odor pulses evoked fast oscillations; lengthy pulses evoked first fast, then slow oscillations. Normalized, average spectrograms from 18 trials obtained from 6 animals with 3 trials each (see Experimental Procedures). Black horizontal bars above each spectrogram: odor pulses.

(D) Power spectra of oscillatory LFP responses averaged from 22 moths and 8 odors, total of 820 trials. Color brackets: 14 Hz-wide bands used to calculate the total oscillatory powers of fast (red, 30-44 Hz) and slow (blue, 10-24 Hz) oscillations in [E].

(E) Total oscillatory power of fast and slow LFP shifted significantly over lengthy odor pulses. Twenty trials tested for each odor were averaged before pooling, mean±SE. n=41; 2-way ANOVA: $f_{window}(2)=26.62$, $P<0.0001$ (fast oscillations); $f_{window}(2)=9.09$, $P<0.0003$ (slow oscillations). Asterisks: significant differences (Tukey-Kramer multiple comparisons).

(F) LFP oscillations in the AL and MB were highly coherent. Left: Example of odor-evoked LFP oscillations recorded simultaneously in the AL and MB; odorant: 1% cyclohexanone (4 s). Areas *a* and *b* are expanded in insets. Horizontal red (0.25-1 s) and blue (1-4 s) bars: times used for coherence analysis at right. Right: Magnitude squared coherence between the AL and MB. Thin black line: coherence of the response shown. Thick black and dotted lines: average coherence and its one standard deviation range (5 AL-MB combinations in 4 preparations, 20 trials each of 2 odorants), respectively.
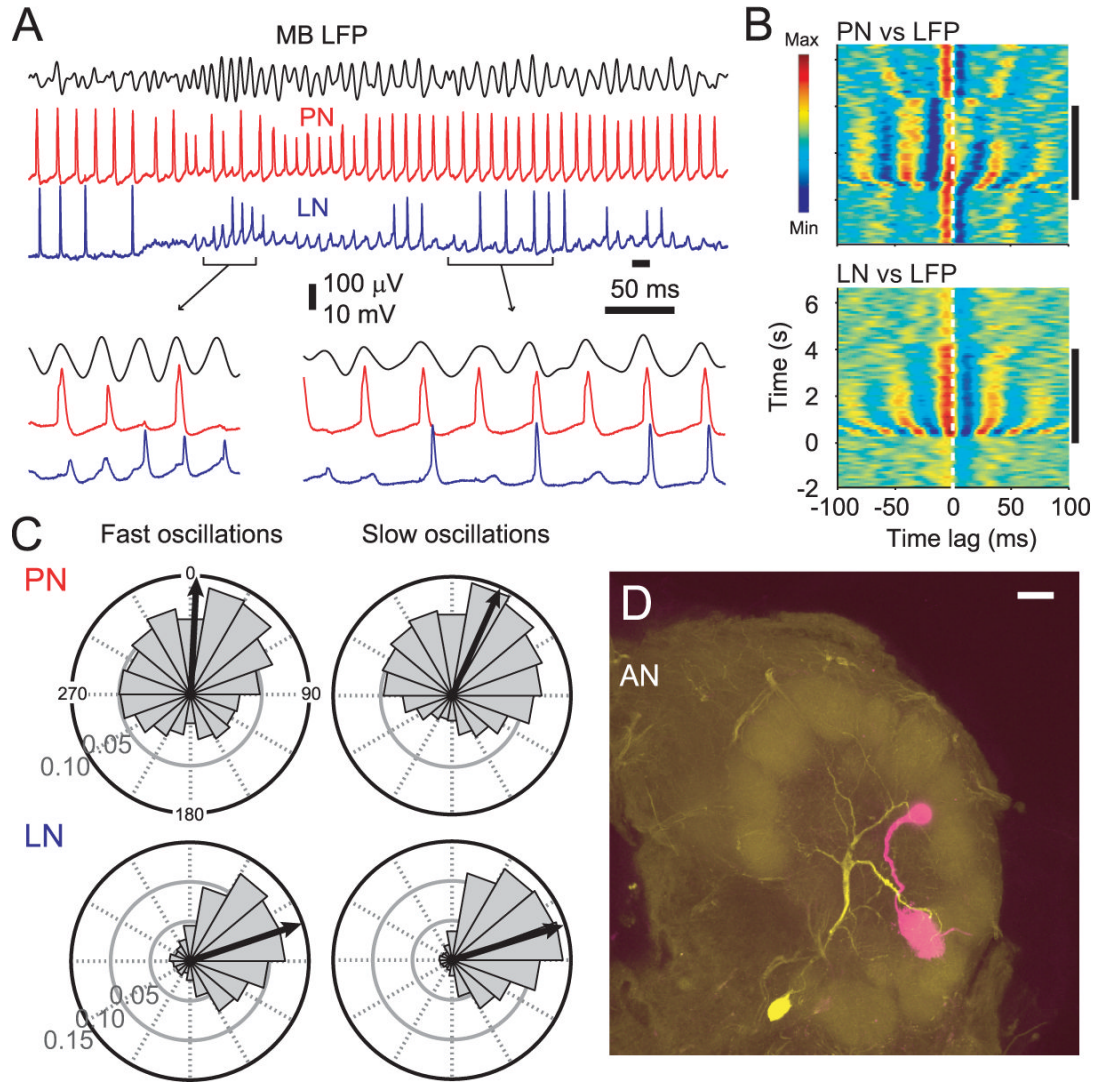
Figure 2. PN and LN responses were strongly phase-locked to the LFP

(A) Example simultaneous intracellular recordings from PN and LN, with LFP recorded in the MB. First 2 s after the odor onset shown; brackets: portions expanded beneath. Odorant: 1% benzyl alcohol.

(B) Subthreshold oscillations: 5-trial average sliding-window cross-correlograms show reliable LFP and subthreshold membrane potential oscillations for the PN (top) and LN (bottom) in [A]. Spikes were clipped. Vertical bars: odor pulses.

(C) Spike-LFP phase relationships: Polar histograms show phase position, relative to LFP, of spikes recorded in PNs (n=14) and LNs (n=30) for fast and slow oscillations. Concentric circles: firing probability. Black arrows: mean direction.

(D) All recorded neurons were filled with dye and later morphologically identified. Example of PN and LN morphology. An Alexa-fluor-633 (red) filled PN and an Alexa-fluor-568 (yellow) filled LN are shown. Scale bar: 50 μm. AN: antennal nerve.
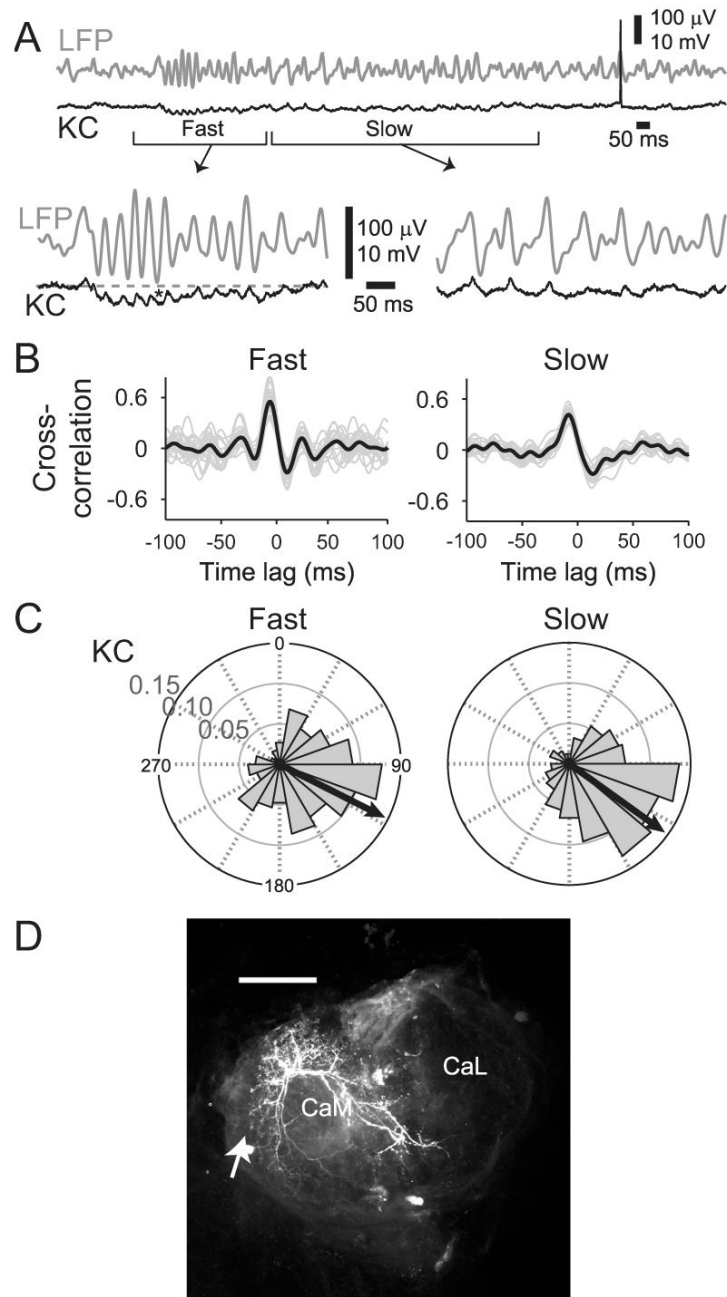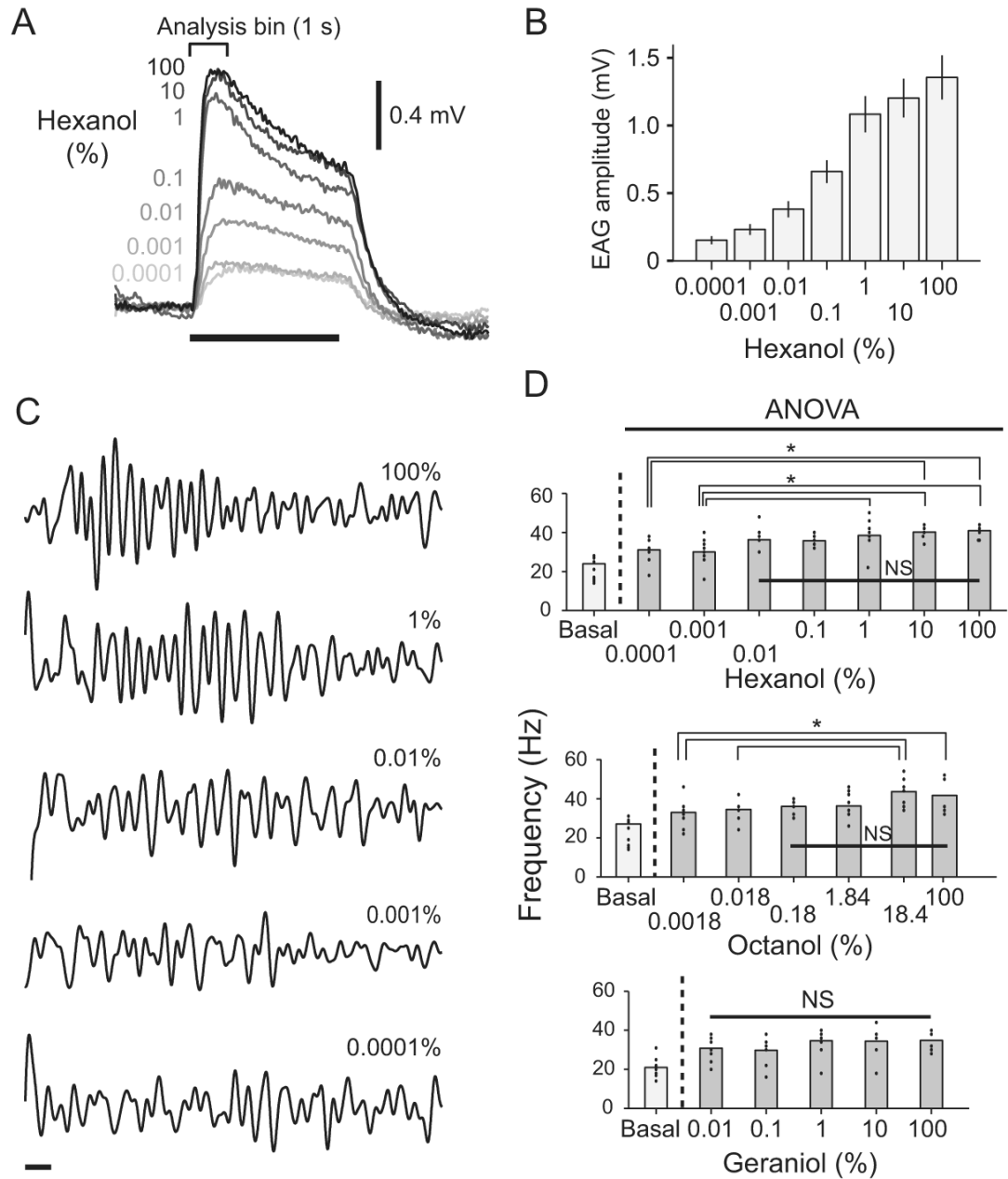
Figure 3. Spiking in KCs is sparse, odor specific, and tightly phase-locked to the LFP
(A) KCs showed odor-elicited subthreshold membrane potential fluctuations that were tightly correlated with LFP oscillations. Example: top, gray: LFP; bottom, black: simultaneous intracellular record of a KC. Bottom: details of fast and slow periods during oscillatory response. Odor: 4 s, 1% benzyl alcohol. Gray broken line: resting potential.
(B) Cross-correlations between LFP oscillations and KC subthreshold activity. Cross-correlation was calculated for times bracketed in [A]. Black lines: correlation for the trial shown in [A]; gray lines: 21 other trials from this cell. All 8 KCs showing subthreshold oscillations revealed similarly-shaped correlation functions, 3 with coefficients >0.3.

(C) Polar histograms show strong phase-locking between spikes in KCs and the LFP oscillations. Histograms show spikes recorded from 20 KCs during fast and slow oscillations. Arrows: mean phase position.

(D) Example of KC morphology; posterior view of MB; KC filled with Alexa Fluor 633. Scale bar: 50 μm. Arrow: soma; CaM: medial calyx; CaL: lateral calyx.

Figure 4. Odor concentration determines oscillation coherence, not frequency

(A) EAG traces revealed total ORN output increased with odor concentration. Example from one antenna; horizontal bar: 4 s.

(B) Summary. EAG amplitude (first 1 s, see bracket in [A]) evoked by a range of odor concentrations. Mean±SE; n=8; 2-way ANOVA: $f_{odor\_concentration}$=16.84, p<0.0001.

(C) Higher concentrations of odor evoked stronger LFP oscillations. Initial portions of the odor response are shown. Scale bar: 50 ms.

(D) The frequency of fast oscillation changed not at all or only slightly across a broad range of odor concentrations. All results are shown (dots); bar graph shows means, n=9. Leftmost bars: basal oscillatory power in absence of odorant. Hexanol: 2-way ANOVA:

$f_{hexanol\_concentration}$=6.16, p<0.001; post hoc Tukey-Kramer tests found small but significant differences between three highest and two lowest concentrations (p<0.05). Octanol: $f_{octanol\_concentration}$=4.98, p<0.001; post hoc tests: significant differences between highest two and lowest two concentrations of octanol (p<0.05); Geraniol: 2-way ANOVA: $f_{geraniol\_concentration}$=1.4, p>0.25, ns.
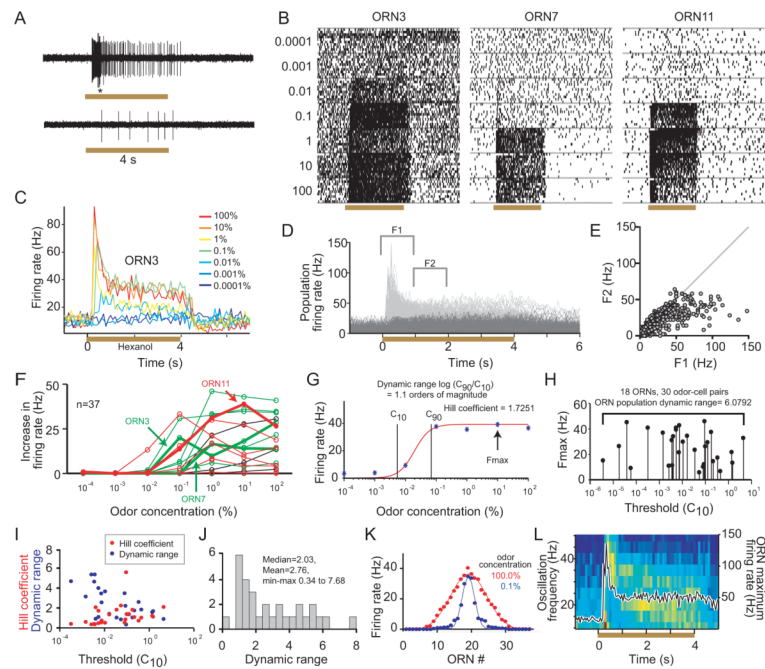
Figure 5. Saturation and adaptation constrained the ORN firing rates

(A) Example extracellular recordings from a sensillum on the antenna show responses to odor pulses (4 s) of 10% hexanol (top) and jasmine oil extract (bottom). Two ORNs were recorded in this sensillum, one with short spikes and sustained firing, and one with large, transiently firing spikes (marked by *). Tan bars: odor pulses.

(B) Spike rasters of three ORNs tested with a wide range of concentrations of hexanol. Blocks of 10 trials for each concentration were tested in random order. Tan bars: odor pulses (4 s).

(C) Instantaneous firing rates of a representative ORN. Spikes were binned (100 ms); spike count in each bin averaged over 10 trials.

(D) The most active ORNs quickly adapted. Instantaneous population firing rate; firing rate averaged over 10 trials for each odor-sensillum combination; 1,011 odor-sensillum combinations (32 sensilla tested with up to 20 odors each). Responses to odor-sensillum combinations were divided into 2 groups based on initial peak firing frequency (>40 Hz: light gray; <40Hz: dark gray). Brackets: 1 s analysis bins used to calculate initial (F1) and late peak (F2) frequencies. For this analysis multiunit activity was included.

(E) Relationship between peak frequencies F1 and F2. Dots under the diagonal line indicate adaptation. Almost all odor-sensillum combinations showing initial spike frequency >40 Hz (F1) underwent adaptation during the stimulus.

(F) Concentration tuning curves for 22 ORNs. Mean firing rates of most ORNs saturated after the odor onset. Red traces: ORNs with firing rates that decreased after the peak concentration; Green traces: ORNs with firing rates that saturated after the peak concentration.

(G) ORN concentration response curves were fit with the Hill equation. Example: ORN22, tested with different concentrations of hexanol. Parameters (C_{10}, C_{90}, Hill coefficient, F_{max}) in panels H-J were obtained from this fitting.

(H) Lack of correlation between maximum firing rates (F_{max}) and the thresholds (C_{10}) of individual ORNs. Response thresholds (C_{10}) spanned about 6 orders of magnitude, indicating our sample of ORNs, as a population, offered a wide dynamic range. Only responsive odor-ORN combinations (n=25, >5 Hz change in mean firing rate during odors) were included in this analysis.

(I) Hill coefficient (red) and dynamic range (blue) as function of threshold. ORNs responding to low concentrations typically showed low Hill coefficients and relatively wide dynamic ranges.

(J) Histogram of Hill coefficients. Most ORN-odor combinations showed Hill coefficients >1, indicating a dynamic range <2 orders of magnitude.

(K) Firing rates in the ORN population followed Gaussian distributions. The numbers of spikes in the first 1 s of odor responses (indicated by colored dots) were counted in 37 ORNs tested with hexanol. The ORN firing rates were fit with Gaussian distributions (colored lines). As the odor concentration increased, the width of the distribution (sigma) broadened but the height of the distribution remained about the same. All odor concentrations evoked responses with Gaussian distributions.

(L) Frequency of MB-LFP oscillations changed in parallel to the odor input (1% hexanol) to the AL network. Odor input: firing rate of the most active ORN (at each 50 ms time slice across 22 ORNs). Power spectrogram: average of 9 preparations.
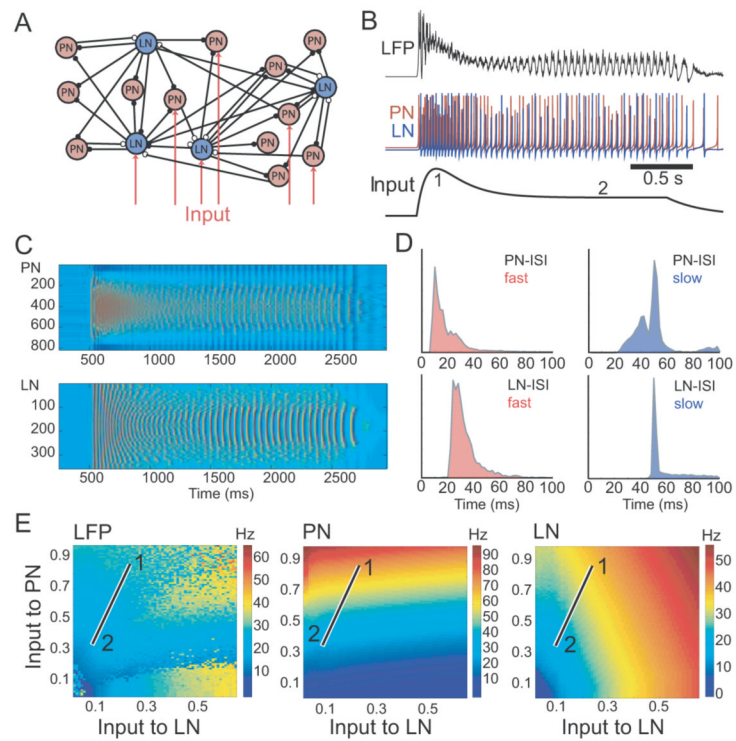
Figure 6. Odor evoked oscillations in model of moth AL

(A) Full-scale, map-based model included randomly connected populations of 820 PNs and 360 LNs. Odor pulse input was simulated by external currents delivered to a subset of neurons.

(B) Amplitude of the input was set to resemble the EAG (bottom). LFP (top) and neuronal (middle) responses resembled those recorded *in vivo*. The input to the model was tuned to match results of our physiological recordings and corresponded to points '1' and '2' in the parameter space shown in [E].

(C) Raster plots show spikes in all PNs (top) and all LNs (bottom) evoked by one odor pulse (applied from 500-2500 ms).

(D) Interspike interval (ISI) distributions during fast and slow phases of LFP oscillations. Many PNs fired two spikes in a single oscillatory cycle (ISI < 25 ms during fast and ISI < 50 ms during slow phase); LN frequency was typically limited to the LFP frequency.

(E) Frequency of LFP, PN and LN oscillations as a function of input from ORNs to PNs and LNs. Sweeping the points between '1' and '2' in parameter space mimicked the ISI distribution (compare [D] and Figure S7) and the abrupt change in oscillatory frequency (compare [B] and the Figure 1C) we observed *in vivo*.
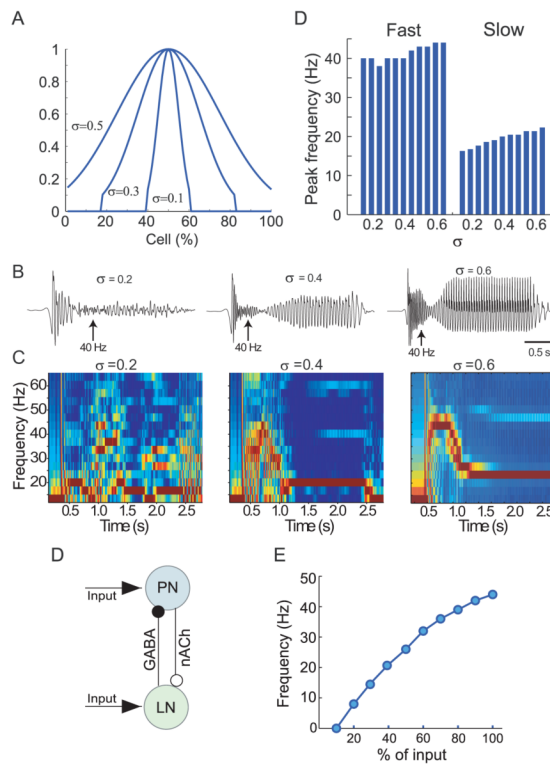
Figure 7. Effect of odor concentration upon LFP frequency in moth AL model
(A) Odor input to the network was simulated by synaptic currents applied to an odor-specific population of PNs and LNs. The size of stimulated population (defined by a Gaussian distribution with width σ; see Figure 5K was varied to simulate different odor concentrations.
(B) Examples of LFP oscillations elicited by three odor concentrations. As *in vivo*, during lengthy odor stimuli the network shifted from fast to slow oscillatory states. LFP was band-pass filtered (5-50 Hz).
(C) Spectrograms of LFP oscillations (those shown in B) for three odor concentrations.
(D) Minimal network consisting of a single PN and LN.
(E) Frequency of oscillations in the minimal network increased sub-linearly as a function of input amplitude.
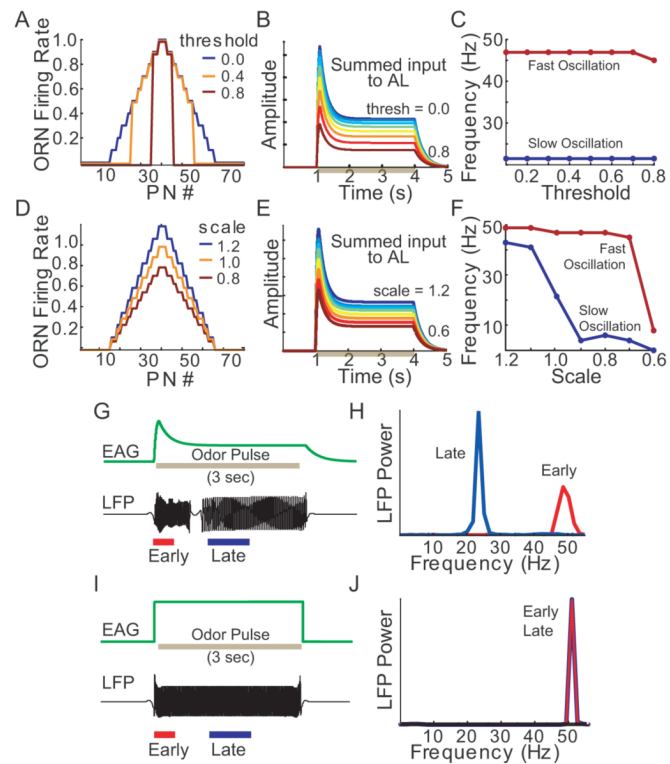
Figure 8. Simplified firing-rate model of the moth AL
(A-C) Varying the width of the distribution of responsive PNs (simulating changes in odor concentration, see Figures 5K and 7A) had no effect on oscillation frequency. (A) Width was varied by adjusting the threshold level for activating PNs. (B) Adjusting the threshold greatly altered overall input to the modeled AL network. (C) The oscillation frequency remained constant despite simulated changes in odor concentration.
(D-F) Varying the height of the distribution of responsive PNs (simulating adaptation in ORNs) caused changes in oscillation frequency. (D) Height was altered by scaling the response intensity of activated PNs. (E) Adjusting the intensity greatly altered overall input to the modeled AL network, as in [B]. (F) The frequency of LFP oscillations decreased when adaptation of ORNs was simulated.
(G-H) Model EAG (green) and LFP response (black) when ORNs are permitted to adapt. Adaptation alone is sufficient to shift the oscillatory frequency (power spectra for early and late oscillations shown in H).
(I-J) Model EAG (green) and LFP response (black) when ORNs are not permitted to adapt. Without adaptation oscillation frequency remains constant (power spectra in J).
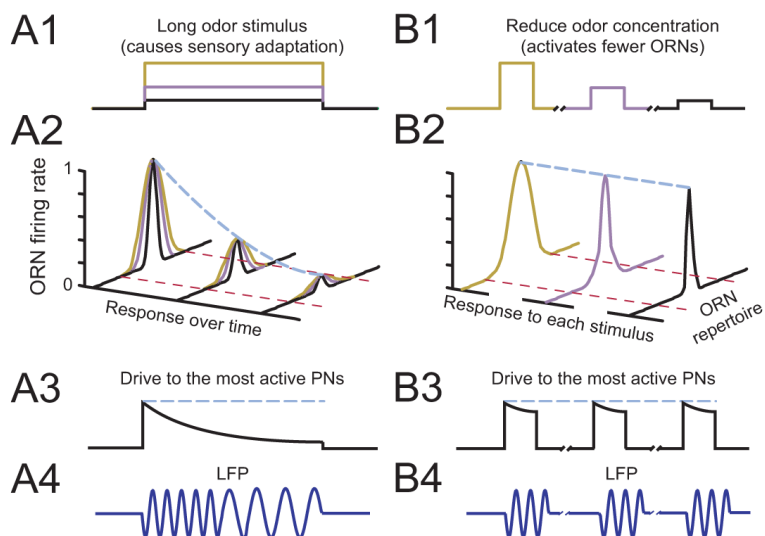
Figure 9. Summary of the mechanism to determine oscillation frequency
(A1) Long odor pulses cause ORNs to undergo sensory adaptation.
(A2) When odor exposure is lengthy, active ORNs adapt, decreasing their firing rates.
(A3) The lower ORN firing rates reduce excitatory drive to PNs.
(A4) As each PN receives less intense input, its firing rate decreases and oscillations slow.
(B1) When odor concentration is reduced, smaller populations of ORNs respond.
(B2) However, the responsive ORNs continue to fire at high rates.
(B3) Thus, the most active PNs continue to receive strong input from responsive ORNs…
(B4) and oscillation frequency remains stable across broad ranges of odor concentration.